Article:
Deng, W, Li, K orcid.org/0000-0001-6657-0522 and Deng, J (2018) Event-triggered H∞ position control of receiver coil for effective mobile wireless charging of electric vehicles. Transactions of the Institute of Measurement and Control, 40 (14). pp. 3994-4003. ISSN 0142-3312

https://doi.org/10.1177/0142331217739084

Event-triggered $H\infty$ position control of Receiver coil for effective mobile wireless charging of electrical vehicles

Weihua Deng[1]**, Kang Li[2], and Jing Deng[2]

[1] College of Electrical Engineering,
Shanghai University of Electric Power, Shanghai, 200090, China
[2] School of Electronics, Electrical Engineering and Computer Science,
Queen's University Belfast, Belfast, BT9 5AH, UK

Abstract. The emergence of dynamic wireless charging (DWC) technologies bring about new possibilities of on-road in-time charging of electric vehicle (EV) in solving the battery bottleneck for the mass roll-out of EVs worldwide. In this new area, the charging efficiency is one of the most important issues to be addressed for on-road wireless charging. Yet, most current researches mainly focus on the electronics power design of the charging system, little has been done on improving the charging efficiency through real-time mechanical control. In this paper, a switch control strategy based on the event-triggered mechanism is first proposed, to improve the charging efficiency when the EV moves along the power supply road track. An $H\infty$ control problem is formulated and the sufficient stabilization criteria is derived in the form of linear matrix inequality (LMI) when the EV derails from the effective charging range. The numerical simulation confirms that the proposed control approach outperforms the general state feedback control (GSFC). The developed control strategy is applied to controlling a newly built EV wireless charging test platform with desirable control performance.

Key words: Electric vehicles, Event-triggered control (ETC), $H\infty$ performance, EV wireless charging platform

1 Introduction

Electric vehicles (EVs) (Miller , 2014) have gained rapid development worldwide in recent years. Indeed, EVs have many advantages such as reducing the consumption of fossil fuels, reducing pollutant emissions, and exploring a broader utilization of the electric energy generated from clean, renewable energy resources. However, the mass roll-out of electric vehicles face a great challenge in battery charging (He and Venkatesh , 2012) and it is just a continuous and challenging problem in the near future. The charging of (pure battery powered) electric vehicles can generally be classified into two categories: plug-in wired (Wang and Chau , 2016, Wayes and Walid , 2012) and contactless (Ko and Young , 2013, Esteban and Sid , 2015, Buja and Bertoluzzo , 2016, Lukic and Pantic , 2013). The plug-in wired charging is currently the most common approach and EVs can be charged at home or charging stations. But this approach may be inconvenient for those whose homes have no charging devices or being far from a fixed charging point. A recent emerging technology, namely, inductive power transfer (IPT) (Covic and Boys , 2013) has been introduced, which charges the EVs by means of contactless or wireless power transfer. The power transmitter terminal is usually placed below the road surface of a dedicated parking deck, the bus stop or the highway, and the power receiver terminal is often attached to the underpan of the EV. The process of charging is either statical or dynamical depending on the specific environment and demands. For example, the car park and private garage can be regarded as the places for stationary or static wireless charging. In the public transportation such as highways and dedicated lines for buses and trains can be chosen as the environment for mobile or dynamic wireless charging. The application of dynamic wireless charging (Choi and Gu , 2015, Chen and Nagendra , 2015, Liu and Huang , 2016) is attractive because it can save time and relieve range anxiety. But this technique is not yet used widely in practice because of its immaturity. A key issue that has a direct impact on the charging efficiency is the ability to have tight alignment between the receiver coil and the transmitter coil as shown in Fig. 1 in the process of dynamic wireless charging. The misalignment will lead to

** Corresponding author: Weihua Deng, Email: dwh197859@126.com

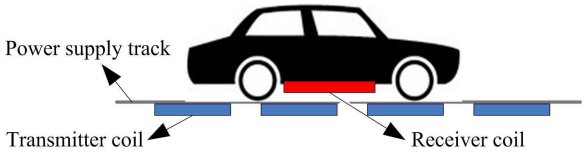

Fig. 1. EV dynamic wireless charging on the power supply track

the decrease of the coupling factor between the receiver coil and the transmiter coil. Accordingly the charging efficiency may significantly decrease. It is therefore important to keep the relative position of the both coils unchanged. The majority of researches on this latest technology mainly focus on the magnetic topologies and power electronics designs (Miller and Jones , 2015, Choi and Gu , 2014, Lee and Pantic , 2014, Covic and Boy , 2013, Zaheer and Neath , 2017). These techniques help both coils to possess wider tolerances for misalignment, yet they may be costly to implement and some technical challenges such as stability are yet to overcome. In this paper, we propose to apply simpler monitoring and mechanical control approaches to assist alignment automatically. This approach can significantly reduce the cost and simplify the design of magnetic and electronic circuits. To date, the mechanical control problems relating to the dynamic wireless charging are rarely researched in the literature and is still at the early stage of development. To achieve mechanical control of the mobile wireless charging still face a few technical challenges which are to be addressed in the paper.

Consider the on-road wireless charging, the driver drives the vehicle along designated road/track which can provide wireless power transfer to charge the EV battery. As illustrated in Fig. 1, many segments of track transmitter coil (in blue) are placed below the road surface to transmit power to the receiver coil under the EV (in red), and these segments of coils beneath the road are separated by a constant distance. The battery in car can be charged as the receiver coil receives the transmitted power. In practice the EV in motion may not exactly follow the charging track. There are two deviation scenarios. The first is a minor deviation from the track coil but within the effective range. This is a normal status, and electronics design can sufficiently solve the charging efficiency for such minor misalignment. While the second scenario is where the deviation is significant enough that the charging efficiency is significantly reduced. This is called the abnormal status. Fig. 2 illustrates different relative positions of the two coils. The receiver coil on the left of Fig. 2 is within the effective range and it belongs to the normal case, while the other two are not within the effective range and thus the charging efficiency will be inevitably decreased. In practice, it does not need to be controlled when the deviation is relatively small because the received power above the effective range is almostly the same, while a large deviation must be adjusted in time. So it is important to explore a control approach which can activate the control action according to the deviation. Thus it can not only guarantee the dynamic wireless charging efficiency but also avoid the redundant control input. This is the first challenge for the design of the mechanical control of the dynamic wireless charging system. On the other hand, it is impossible to adjust the positon of the transmitter coil because it is fixed below the road surface. So only the receiver coil can be controlled. It is therefore to design a light mechanical device which can connect the EV and the receiver coil. The mechanical device can allow the receiver coil move flexibly to keep the alignment of the both coils under control. This is the second challenge for the applicaton of the mechanical control.

Aiming to tackle the above two challenges, the main contributions of this paper are summarized as follows. First a theory frame is proposed to analyze the dynamic behaviour of the EV when it is running along the track as shown in Fig. 1. The switched system approach is used to model the relationship between relative lateral deviation of the both coils and the receiving power of the EV. Then an event-triggered control method is used to adjust the deviation. The event-triggered control (Selivanov and Fridman , 2016, Girard , 2015, Zhang and Zheng , 2017) has been studied extensively in recent years, which offers the mechanism to trigger the control action according the specific condition. Secondly a light mechanical equipment is designed to implement the mechnical control. The mechanical device consists of a conveyor belt, a stepper motor and a plastic supporting board, which is easy to connect the car body and the receiver coil. The receiver coil can move following the supporting board which is driven by the stepper motor.

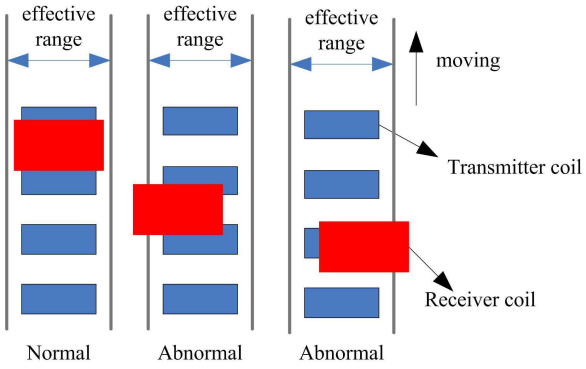

Fig. 2. Top view of relative position of receiver coil and track coil

The rest of this paper is structured as follows. Section II presents a mathematical modeling of the EV dynamic wireless charging process. The proposed the event-triggered control strategy and design algorithm are also given in Section II. The sufficient condition for solving controller gains is given in form of the LMIs in Section III. In Section IV, a simulation case study is used for illustrating the proposed control approach. The mechanical device design and controller realization are introduced in experimental results of Section V. Finally, Section VI concludes the paper.

2 Problem formulation

2.1 System model

The receiver coil is installed above the supporting board of the mechanical device which will be introduced in detail in the experiment section. The whole device is called receiver in brief. The receiver can detect the distance between the center of the receiver coil and the left boundary of the effective range automatically and adjust its position when the receiver coil is not in the effective range. The relative position is shown in Fig. 3. The length of the effective range is L and the distance between the center of receiver coil and the left boundary of the effective range is $d(k)$. $d(k) \in \left[d_{\min}, d_{\max}\right]$, $d(k) \in \left[0, d_{\min}\right]$ and $d(k) \in \left[d_{\max}, L\right]$ are defined respectively as the three status, and $d_{\min} \in \left[0, \frac{L}{2}\right], d_{\max} \in \left[\frac{L}{2}, L\right]$ are the left border and right border of the effective range respectively.

The power which the receiver coil collected is decided by a number of factors, for example, the track coil working frequency, the number of track coil, and the relative position between the receiver coil and track coil, etc. In this paper, we only focus on the impact of the random movement of EV on the receiving power. $d(k)$ is a variable which may be disturbed by $w(k)$, and $w(k)$ is a stochastic factor such as driver behavior or road status. Here $\Delta d(k)$=$d(k) - L/2$ as shown in Fig. 3 represents the relative distance between the center positions of the receiver coil and the effective range. And $\Delta P(k)$ stands for the received power variation which is induced by $\Delta d(k)$. We will study the relation of these two variables. Furthermore, if the control $u_{\theta(k)}(k)$ is used to eliminate the influence of $\Delta d(k)$, then the system can be modeled as a linear discrete time switched system as shown in Fig. 4.

The following dynamic model can be derived from Fig. 4

$$\begin{aligned} x(k+1) &= Ax(k) + Bu_{\theta(k)}(k) + \tilde{B}w(k) \\ y(k) &= Cx(k) \end{aligned} \tag{1}$$

where

$$x(k) = \begin{bmatrix} \Delta d(k) \\ \Delta P(k) \end{bmatrix}, A = \begin{bmatrix} a & 0 \\ \bar{b} & \bar{a} \end{bmatrix}, B = \begin{bmatrix} b \\ \bar{b} \end{bmatrix}$$
$$\tilde{B} = \begin{bmatrix} b \\ 0 \end{bmatrix} C = \begin{bmatrix} 0 & 1 \end{bmatrix}$$

and $u_{\theta(k)}(k)$ is a switched controller which will be introduced in next subsection.

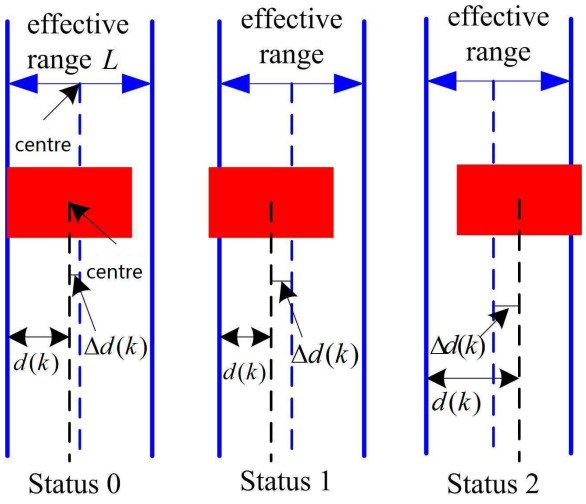

Fig. 3. The different status of $d(k)$

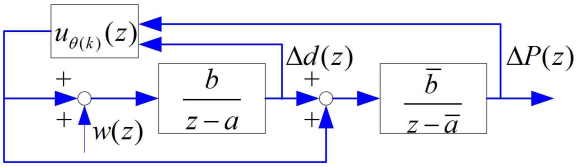

Fig. 4. Dynamic model of the switched control system

2.2 Switch control based on an event-triggered

In practice, the three status in Fig. 3 will switch randomly, depending on various stochastic factors. The status 0 does not need to be controlled. The status 1 and 2 need to be adjusted in time. The controller $u_{\theta(k)}(k)$ will switch according to the switching signal $\theta(k)$. The signal $\theta(k)$ is defined as

$$\theta(k) : k \geq 0 \rightarrow \Omega := \{1, 2, \ldots, N\} \tag{2}$$

and it will enable one and only one controller among N known controllers $\mathrm{U} := u_i, \forall i \in \Omega$ at each instant of time $k \geq 0$. Here $N = 2$ and the switch signal is $\Delta d(k)$. If $\Delta d(k)$ is defined as the sample space $D = \{\Delta d(k) \in (-\frac{L}{2}, \frac{L}{2})\}$, and the whole sample space is partitioned into four subspaces

$$\begin{aligned} D_1 &= \{\Delta d(k) \in (-\tfrac{L}{2}, d_{\min} - \tfrac{L}{2}]\} \\ D_2 &= \{\Delta d(k) \in (d_{\min} - \tfrac{L}{2}, 0]\} \\ D_3 &= \{\Delta d(k) \in (0, d_{\max} - \tfrac{L}{2}]\} \\ D_4 &= \{\Delta d(k) \in (d_{\max} - \tfrac{L}{2}, \tfrac{L}{2})\} \end{aligned} \tag{3}$$

then the controller will switch in the following two subcontrol modes

$$u_{\theta(k)}(k) = \begin{cases} u_1(k), D_1 \cup D_2 \\ u_2(k), D_3 \cup D_4 \end{cases}. \tag{4}$$

Furthermore $u_{\theta(k)}(k)$ can be described as

$$u_{\theta(k)}(k) = \delta(k)u_1(k) + (1 - \delta(k))u_2(k) \tag{5}$$

where k is the discrete time and

$$\delta(k) = \begin{cases} 1, D_1 \cup D_2 \\ 0, D_3 \cup D_4 \end{cases}. \tag{6}$$

As aforementioned, status 0 does not need control. When the control action is triggered after switching on one of its subcontrol modes depending on the specific trigger condition $\theta_i(k), i = 1, 2$ defined as

$$\begin{array}{l} \theta_1(k) : k \geq 0 \rightarrow \Theta_1 := \{1, 2\} \\ \theta_2(k) : k \geq 0 \rightarrow \Theta_2 := \{1, 2\} \end{array} \tag{7}$$

and the corresponding controller under the corresponding submode is

$$\begin{array}{l} K_{1\theta_1(k)}(k) = \begin{cases} K_{11},\, D_1|B_1 \\ K_{12},\, D_2|B_1 \end{cases} \\ K_{2\theta_2(k)}(k) = \begin{cases} K_{21},\, D_4|B_2 \\ K_{22},\, D_3|B_2 \end{cases} \end{array} \tag{8}$$

where

$$\begin{array}{l} B_1 = D_1 \cup D_2 \\ B_2 = D_3 \cup D_4 \end{array}.$$

It means that one and only one among $M = 2$ known controllers $K := K_{ij}, \forall j \in \Theta_j$ under the ith sub control mode is triggered respectively when the corresponding triggering condition is satisfied. It needs to be clear that $K_{12} = 0, K_{22} = 0$ when the EV is on the status 0. Now the controller can be described as

$$\begin{array}{l} u_{\theta(k)}(k) = \delta(k)((\delta'(k)K_{11}x(k) + (1 - \delta'(k))K_{12}x(k)) \\ +(1 - \delta(k))(\delta''(k)K_{21}x(k) + (1 - \delta''(k))K_{22}x(k)) \end{array} \tag{9}$$

where

$$\delta'(k) = \begin{cases} 1,\, D_1|B_1 \\ 0,\, D_2|B_1 \end{cases}, \delta''(k) = \begin{cases} 1,\, D_4|B_2 \\ 0,\, D_3|B_2 \end{cases}. \tag{10}$$

Then the closed-loop control system can be obtained from (1) and (9)

$$\begin{array}{l} x(k+1) = Ax(k) + \delta(k)\delta'(k)BK_{11} \\ +(1 - \delta(k))\delta''(k)BK_{21} + \tilde{B}w(k) \\ y(k) = Cx(k) \end{array} \tag{11}$$

The next step is how to find the proper controller gains K_{11}, K_{21}.

3 Main results

In this section, we will develop an event-triggered switch controller to make the closed-loop system (11) satisfying:

1) system (11) with $w(k) = 0$ is asymptotically stable.
2) under the zero initial conditon, $\|y(k)\|^2 < \gamma^2\|w(k)\|^2$, for any nonzero $w(k) \in L_2[0, \infty]$ and a prescribed $\gamma > 0$.

We first construct the Lyapunov functional candidate as follows

$$V(k, x(k)) = x^T(k)Px(k) \tag{12}$$

where $P > 0$. Then its difference along the solution of the system (11) can be obtained as follow

$$\begin{array}{l} \Delta V(k, x(k)) = V(k+1, x(k+1)) - V(k, x(k)) \\ = x^T(k+1)Px(k+1) - x^T(k)Px(k) \\ = [A(k)x(k) + w(k)]^T P[A(k)x(k) + w(k)] \\ -x^T(k)Px(k) \end{array} \tag{13}$$

where

$$A(k) = A + \delta(k)\delta'(k)BK_{11} + (1 - \delta(k))\delta''(k)BK_{21}.$$

It is obvious that $\delta(k)$, $\delta'(k)$ and $\delta''(k)$ in $A(k)$ are random variables and their values are decided by $\Delta d(k)$. We will apply an expectation operator in Deng and Li (2013), Peng and Ma (2017), to deal with this problem. To use the technique, the following preliminaries are introduced first.

If the probability of $\Delta d(k)$ in (3) is assumed as follows

$$p(D_1) = p_1, p(D_2) = p_2, p(D_3) = p_3, p(D_4) = p_4, \tag{14}$$

then the following can be obtained based on the conditional probability formula

$$\begin{array}{l} p(B_1) = \sum\limits_{i=1}^{4} p(D_i)p(B_1|D_i) = p_1 + p_2 \\ p(B_2) = \sum\limits_{i=1}^{4} p(D_i)p(B_1|D_i) = p_3 + p_4 \end{array}. \tag{15}$$

Thus usig the law of total probability, yields

$$\begin{array}{l} p(D_2|B_1) = \frac{p(D_2B_1)}{p(B_1)} = \frac{p_2}{p_1+p_2} \\ p(D_1|B_1) = \frac{p(D_1B_1)}{p(B_1)} = \frac{p_1}{p_1+p_2} \\ p(D_3|B_2) = \frac{p(D_3B_2)}{p(B_2)} = \frac{p_3}{p_3+p_4} \\ p(D_4|B_2) = \frac{p(D_4B_2)}{p(B_2)} = \frac{p_4}{p_3+p_4} \end{array}. \tag{16}$$

Based on the above analysis, the probabilities of several variables that are used in the expectation operation are listed in table 1 based on (6), (10), (14)-(16).

Table 1. The list of probability values.

Item	Probability
$\delta(k)\delta'(k)$	$\frac{p_1}{p_1+p_2}$
$(1-\delta(k))\delta''(k)$	$\frac{p_4}{p_3+p_4}$
$\delta(k)\delta'(k)\delta''(k)(1-\delta(k))$	0

Now we apply the expectation operator to the two sides of (13) on $x(k)$ simultaneously and use table 1 yielding

$$\begin{array}{l} \mathrm{E}(\Delta V(k, x(k))|x(k)) \\ = \begin{bmatrix} x(k) \\ w(k) \end{bmatrix}^T \begin{bmatrix} \Lambda_1 & \Lambda_2 \\ * & \Lambda_3 \end{bmatrix} \begin{bmatrix} x(k) \\ w(k) \end{bmatrix} - x^T(k)Px(k) \end{array} \tag{17}$$

where

$$\begin{array}{l} \Lambda_1 = \Lambda_{11}^T P\Lambda_{11} + \Lambda_{12}^T P\Lambda_{12} + \Lambda_{13}^T P\Lambda_{13} \\ +\Lambda_{14}^T P\Lambda_{14} - A^T PA \\ \Lambda_2 = \Lambda_{11}^T P\tilde{B} + \Lambda_{12}^T P\tilde{B} - A^T P\tilde{B} \\ \Lambda_3 = \tilde{B}^T P\tilde{B}, \Lambda_{11} = A + p_{12}BK_{11}, \Lambda_{12} = A + p_{34}BK_{21} \\ \Lambda_{13} = \sqrt{p_{12}(1-p_{12})}BK_{11}, \Lambda_{14} = \sqrt{p_{34}(1-p_{34})}BK_{21} \\ p_{12} = \frac{p_1}{p_1+p_2}, p_{34} = \frac{p_4}{p_3+p_4} \end{array}.$$

From (17), we have

$$\begin{array}{l} \mathrm{E}(\Delta V(k, x(k))|x(k)) + y^2(k) - \gamma^2 w^2(k) \\ = \begin{bmatrix} x(k) \\ w(k) \end{bmatrix}^T \begin{bmatrix} \Lambda_1 - P + C^T C & \Lambda_2 \\ * & \Lambda_3 - \gamma^2 \end{bmatrix} \begin{bmatrix} x(k) \\ w(k) \end{bmatrix} \end{array} \tag{18}$$

Then if the following matrix inequality

$$\begin{bmatrix} \Lambda_1 - P + C^T C & \Lambda_2 \\ * & \Lambda_3 - \gamma^2 \end{bmatrix} < 0 \tag{19}$$

holds, then $\mathrm{E}(\Delta V(k,x(k))|x(k))+y^2(k)-\gamma^2 w^2(k)<0$. It is also easy to prove that $\mathrm{E}\left\{\sum_{k=0}^{\infty}\Delta V(k,x(k))|x(k)\right\}+\sum_{k=0}^{\infty}y^2(k)-\gamma^2\sum_{k=0}^{\infty}w^2(k)<0$. Under zero initial condition $x(0)=0$, we have $\|y(k)\|^2<\gamma^2\|w(k)\|^2$ for any nonzero $w(k)\in L_2[0,\infty]$. On the condition that $w(k)=0$, then there exists a scalar $\lambda>0$ such that $\sum_{k=0}^{\infty}\mathrm{E}(\Delta V(k,x(k))|x(k))<-\lambda\sum_{k=0}^{\infty}\|x(k)\|^2$, based on which we can get $\mathrm{E}(\|x(k)\|^2)\to 0, k\to\infty$. Based on the above analysis, the system (11) is asymptotically stable with an $H\infty$ performance.

Now we have deduced sufficient condition (19) to find the controller gains K_{11}, K_{21}. Since there are some coupling items in (19), it is difficult to directly solve the gains. In the following, linear matrix inequality (LMI) approach will be applied to solve (19). After applying the Schur complement operator to (19), we have

$$\begin{bmatrix} \Upsilon_{11} & \Upsilon_{12} & \tilde{\Upsilon}_{13} & \tilde{\Upsilon}_{14} & \tilde{\Upsilon}_{15} & \tilde{\Upsilon}_{16} \\ * & \Upsilon_{22} & \Upsilon_{23} & \Upsilon_{24} & \Upsilon_{25} & \Upsilon_{26} \\ * & * & \tilde{\Upsilon}_{33} & \Upsilon_{34} & \Upsilon_{35} & \Upsilon_{36} \\ * & * & * & \tilde{\Upsilon}_{44} & \Upsilon_{45} & \Upsilon_{46} \\ * & * & * & * & \tilde{\Upsilon}_{55} & \Upsilon_{56} \\ * & * & * & * & * & \tilde{\Upsilon}_{66} \end{bmatrix}<0 \tag{20}$$

where

$$\begin{aligned}
&\Upsilon_{11}=-P+C^TC-A^TPA, \Upsilon_{12}=-A^TP\tilde{B}\\
&\tilde{\Upsilon}_{13}=A^TP+p_{12}\bar{P}_1^T, \tilde{\Upsilon}_{14}=A^TP+p_{34}\bar{P}_2^T\\
&\tilde{\Upsilon}_{15}=\sqrt{p_{12}(1-p_{12})}\bar{P}_1^T, \tilde{\Upsilon}_{16}=\sqrt{p_{34}(1-p_{34})}\bar{P}_2^T\\
&\Upsilon_{22}=-\tilde{B}^TP\tilde{B}-\gamma^2, \Upsilon_{23}=\Upsilon_{24}=\tilde{B}^T\\
&\tilde{\Upsilon}_{33}=\tilde{\Upsilon}_{44}=\tilde{\Upsilon}_{55}=\tilde{\Upsilon}_{66}=-P^{-1}\\
&\Upsilon_{25}=\Upsilon_{26}=\Upsilon_{34}=\Upsilon_{35}=0\\
&\Upsilon_{36}=\Upsilon_{45}=\Upsilon_{46}=\Upsilon_{56}=0.
\end{aligned}$$

Pre- and post multiplying both sides of (20) with $diag\{I,I,P,P,P,P\}$ and its transpose, respectively, and introducing $\bar{P}_1=PBK_{11}, \bar{P}_2=PBK_{21}$, yielding (21),

$$[\Upsilon_{ij}]<0 \tag{21}$$

where

$$\begin{aligned}
&\Upsilon_{13}=A^TP+p_{12}\bar{P}_1^T, \Upsilon_{14}=A^TP+p_{34}\bar{P}_2^T\\
&\Upsilon_{15}=\sqrt{p_{12}(1-p_{12})}\bar{P}_1^T, \Upsilon_{16}=\sqrt{p_{34}(1-p_{34})}\bar{P}_2^T.
\end{aligned}$$

It is obvious that (21) is a LMI which is easy to be solved using the LMIs toolbox in Matlab.

Based on the preceding analysis, the following theorem can be established.

Theorem 1: For some given positive constants p_1,p_2,p_3,p_4 and γ, the system (11) is asymptotically stable with a prescribed disturbance attenuation level γ, if there exist matrices $P>0$ and matrix $\bar{P}_1,\bar{P}_2$ wtih appropriate dimensions such that linear matrix inequality (21) is satisfied. The switched controller gains $K_{11}=B\backslash(P^{-1}\bar{P}_1), K_{21}=B\backslash(P^{-1}\bar{P}_2)$, where $\backslash$ represents matrix division.

Remark 1: If the controller $u_{\theta(k)}(k)$ in (1) is replaced by $u(k)=Kx(k)$, then event-triggered control can be reduced to the general state feedback control problem. In simulaiton section, we will make a comparison for the two control approaches.

4 Numerical Simulation analysis

In this section, the numerical simulation is used to illustrate the efficacy of the method developed in the above sections. The simulation is made by use of the simulink and LMI toolbox in MatlabR2013a under Windows10 environment.

4.1 Model selection

To proceed to the numerical simulation, the first step is to choose the model parameters to reflect as closely as possible the movement of an EV on the road. As pointed out in the modelling secton, $\Delta P(k)$ is decided uniquely by $\Delta d(k)$, and $\Delta d(k)$ may be disturbed by $w(k)$. The EV will normally remain at the current status if it is not affected by external factor including random diturbance and control. For example, if the EV leaves out of the effective range of a track transmitter coil, then it will not return without any control action. Further, if there is no disturbance, then the EV will stay at the current position. This implies that the EV is in a marginally stable. According to the above analysis, the model parameters are chosen as

$$A = \begin{bmatrix} 1 & 0 \\ 1 & 1 \end{bmatrix}, B = \begin{bmatrix} 1 \\ 1 \end{bmatrix}, \tilde{B} = \begin{bmatrix} 1 \\ 0 \end{bmatrix}, C = \begin{bmatrix} 0 & 1 \end{bmatrix}.$$

4.2 $H\infty$ performance analysis

In addition, the probability of the EV leaves the effective range depends on the random disturbance. Here we choose two of disturbance values

$$w_1(k) = \begin{cases} 0.05 : k = 2.5, 6.5 \\ 1 : k = 4.5, 10.5 \\ -0.08 : k = 8.5 \\ 0 : k = others \end{cases}$$

and

$$w_2(k) = \begin{cases} 0.05 : k = 2.5, 6.5 \\ 1 : k = 4.5, k = 10.5 \\ -0.08 : k = 8.5 \\ 0.5 : k = 11 \\ -1 : k = 5, k = 13 \end{cases}$$

where disturbance $w_1(k)$ is smaller than $w_2(k)$. The corresponding probability values $\{p_1 = 0, p_2 = 12/15, p_3 = 1/15, p_4 = 2/15\}$ and $\{p_1 = 2/15, p_2 = 9/15, p_3 = 1/15, p_4 = 3/15\}$ can be obtained according to the disturbance values. The probability of the EV leaves the effective range depends on the random disturbance. The different disturbance values will produce different probability values. And the corresponding probability values can be obtained according to the disturbance values. By simply calculations, one can obtain the table 2 which shows the $H\infty$ performance of $w(k)$ on $\Delta P(k)$ under different cases. γ^* represents the practical disturbance attenuation level.

Table 2. The practical $H\infty$ performance under different disturbance .

γ^*	$\gamma = 5$	$\gamma = 10$
$w_1(k)$	0.0220	0.0248
$w_2(k)$	0.0089	0.0104

From table 2 it is clear that the practical disturbance attenuation level decreases as the disturbance increases and it increases as the pre-given disturbance attenuation level increases. It illustrates that the disturbance rejection capacity of the control system (11) becomes stronger as the disturbance gets larger. And the practical disturbance attenuation level will change synchronously with the pre-given value. In addition, from the simulation results, it can be seen that the practical disturbance attenuation level under this simulation condition is always smaller than the pre-given level, which confirms the efficacy of the proposed approach.

4.3 Control methods validation

Now both the proposed event-triggered control (ETC) and the general state feedback control (GSFC) are used to control the position deviation $\Delta d(k)$ based on the above model and disturbance. First $L = 1$, $d_{\min} = 0.4$, $d_{\max} = 0.6$ and $D_1 = \{\Delta d(k) \in (-0.5, -0.1]\}, D_2 = \{\Delta d(k) \in$

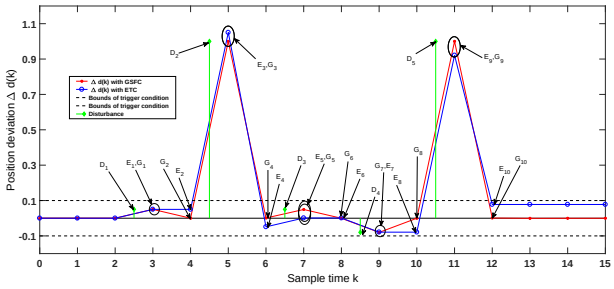

Fig. 5. $\Delta d(k)$ under different control approaches with $w_1(k)$: The sequence { D_i, i=1, 2, 3, 4,5} represents disturbances, the sequence {E_i, i=1, 2, $\cdots$, 10} represents the responses for corresponding disturbance under ETC, and the sequence {G_i, i=1, 2, $\cdots$, 10} represents the responses for correponding diturbances under GSFC.The small deviation caused by disturbance is not controlled under ETC because the trigger condition is not satisfied. On the contrary, any deviation caused by disturbance is alway controlled with GSFC

$(-0.1, 0]\}, D_3 = \{\Delta d(k) \in (0, 0.1]\}, D_4 = \{\Delta d(k) \in (0.1, 0.5)\}$ are selected as the effective range and sample space in (3). Then the trigger condition can be obtained as $\Delta d(k) \in [-0.1, 0.1]$. It means that the receiver coil position will not be adjusted when the trigger condition is not satisfied. In addition, we choose $\gamma = 10$ and $w_1(k)$ as the priscribed $H\infty$ performance and disturbance respectively. Then the controller gains $K_{11} = K_{21} = \begin{bmatrix} -0.9988 & -0.5008 \end{bmatrix}$ can be obtained by solving (21). And (21) is an LMI which can be solved by the lmitoolbox in Matlab. The stability of $\Delta d(k)$ is also shown in Fig. 5 under ETC and GSFC. Three action sequences are shown in Fig. 5. The sequence { D_i, i=1, 2, 3, 4,5} represents disturbances, the sequence {E_i, i=1, 2, $\cdots$, 10} represents the responses for corresponding disturbance under ETC, and the sequence {G_i, i=1, 2, $\cdots$, 10} represents the responses for the correponding diturbances under GSFC. The specific sequences are explained below according to the given disturbance sequence:

- The first disturbance D_1 is introduced with the magnitude 0.05 at k=2.5:
  - k=3: E_1 and G_1 occur and the deviations are increased because of the introduction of disturbance D_1 ;
  - k=4: E_2 occurs and the deviation has no change under ETC because the disturbance is too small and the control action is not activated;
  - k=4: G_2 occurs and the deviation is adjusted back to the equilibrium point zero under GSFC.
- The second disturbance D_2 with the magnitude 1 is produced at k=4.5:
  - k=5: E_3 and G_3 occur and the deviations are increased due to the introduction of the disturbance D_2 ;
  - k=6: E_4 occurs and deviation is adjusted back to the range $[-0.1, 0.1]$ under ETC because the disturbance is too large so that the triggered condition is satisfied;
  - k=6: G_4 occurs and the deviation is adjusted back to the equilibrium point zero under GSFC.
- The third disturbance D_3 occurs and the value 0.05 is produced at k=6.5:
  - k=7: E_5 and G_5 occur and the deviations are increased because of D_3 ;
  - k=8: E_6 occurs and the deviation has no change under ETC because the disturbance is too small and the control action is not activated;
  - k=8: G_6 occurs and the deviation is adjusted back to the equilibrium point zero under GSFC.
- The fourth disturbance D_4 occurs and the value -0.08 is produced at k=8.5:
  - k=9: E_7 and G_7 occur and the deviations are decreased because of D_4 ;
  - k=10: E_8 occurs and the deviation has no change under ETC because the disturbance is too small and the control action is not activated;
  - k=10: G_8 occurs and the deviation is adjusted back to the equilibrium point zero under GSFC.

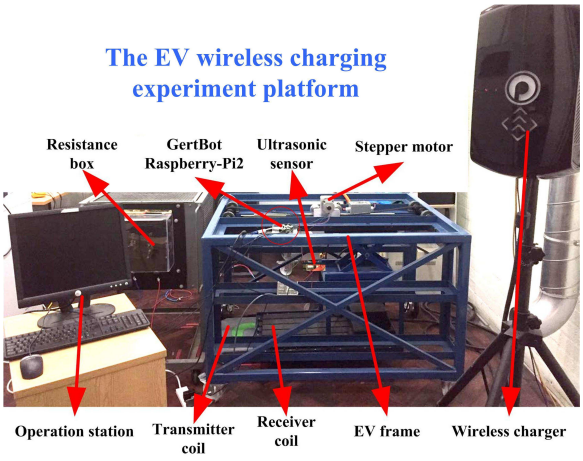

Fig. 6. The EV wireless charging experiment platform

– The fifth disturbance D_5 occurs and the value 1 is produced at k=10.5:
  - k=11: E_9 and G_9 occur and the deviations are increased because of D_5 ;
  - k=12: E_{10} occurs and deviation is adjusted back to the range $[-0.1, 0.1]$ under ETC because the disturbance is too large so that the triggered condition is satisfied;
  - k=12: G_{10} occurs and the deviation is adjusted back to the equilibrium point zero under GSFC.

Based on the above simulation analysis we can see that less control actions are taken under the event-triggered control than the general state feedback control. This explains why we adopt the ETC. Because the power which the EV receives within the effective range is almostly the same. So smaller deviations from the track do not need to be adjusted thus the redundant control actions can be reduced, and less energy are wasted due to unnecessary control actions.

5 Experiment results

In this section, an experimental platform for dynamic wireless charging is designed. The strategy of the event-triggered control is then applied in the experiment. The controller gains in this framework are just the steps of the stepper motor. The steps that the stepper motor should walk in every control process will be computed in real time according to the measurement of the distance by the controller.

5.1 The platform design

An experiment platform is built in the EV laboratory of at Queen's University Belfast as shown in Fig. 6. This platform consists of a wireless charger, a transmitter coil, a receiver coil, a resistance box, a stepper motor and a mechanical device. The wireless charging system is from plugless company. The wireless charging system includes three components: the vehicle adapter, the parking pad, and the control panel. In the experiment of this paper, the vehicle adapter is the receiver coil which is set up under the car frame, and the parking pad is the transmitter coil which is put on the ground. The EV can be modelled by the resistance box and the car frame of the mechanical device. The power received by the resistance box represents the power absorbed from the battery of the EV. The transmitter coil is fixed on the ground as the track coil. The receiver coil is embedded into the supporting board of the mechanical device and the board is driven by the stepper motor. The controller is implemented by the combination of GertBot and Raspberry-Pi 2 and the stepper motor is under the control of GertBot. The control program is coded by Python3.5 in Ubuntu environment.

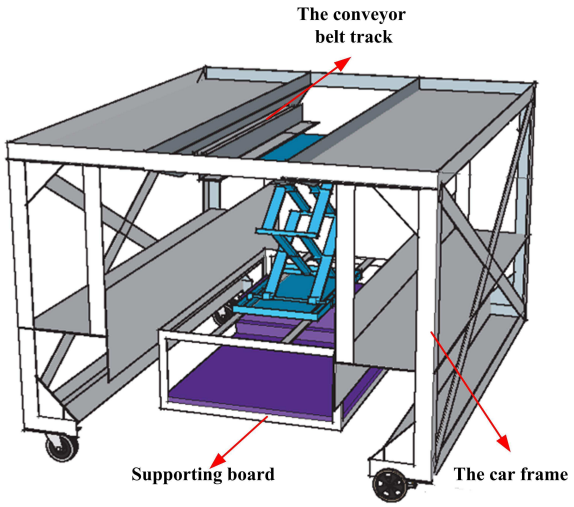

Fig. 7. The frame diagram of the mechanical device

5.2 The mechanical device

As shown in Fig. 7 the mechanical device consists of a car frame, a conveyor belt track and a plastic supporting board. The conveyor belt and the motor are installed on the track. The receiver coil is embedded in the plastic supporting board and can move following the supporting board which is driven by the stepper motor. The mechanical device can not only connect the car body and the receiver coil easily, but also guarantee the flexible movement of the receiver coil under control. In addition, the supporting board of the mechanical device can be adjusted vertically according to different chassis clearance of different EVs, including two different electric vehicles retrofitted at the EV laboratory which will be used in the future study.

5.3 The effective range measurment

The effective range in this experiment was found by measuring the received power distribution of the EV. The received power by the EV is represented by the consuming power of the resistance box in this experiment. The power can be obtained by use of the power equation

$$P = \frac{U^2}{R}$$

where the resistance R can be measured directly but it is difficult to use the online measurement of voltage U in GertBot and raspberryPi because of their limits of rated voltages. So a voltage divider consisting of two resistances (R_s, R_b), of distinctive values is adopted. It is in series connection to the receiver coil. Thus the voltage U in the power equation can be computed by the voltage division formulas. It is thus easy to connect the voltage of the small resistance R_s to the GertBot and raspberryPi. Based on the above design, the power consumption of the reistance box can be fed to the controller in real time. The detailed measurements are shown in Fig. 8. From Fig. 8, we can see that the effective range is 80 cm, i.e., the EV can be effectively charged when the receiver coil is within this range. If the left sides of the receiver coil and the effective range are aligned as shown in Fig. 8, then the power distribution can be measured. Fig. 9 illustrates the received power distribution when the receiver moves from the left bound to the right bound. There are the 5 groups of power values as shown in Fig. 9 and it is clear that they are quite similar when the receiver coil is within the effective range.

5.4 The distance measurment scheme

The distance is measured by an ultrasonic range sensor (HC-sr04) which is installed above the supporting board. The 5 volt power supply for the sensor is provided by J12 pins in the GertBot

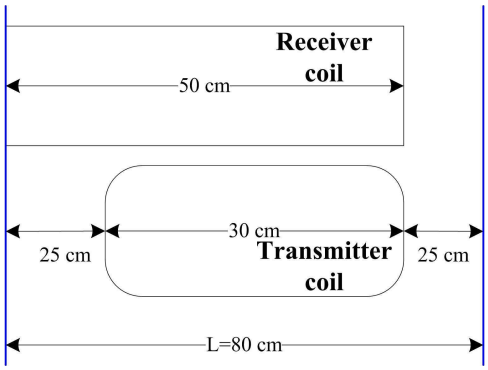

Fig. 8. The real measurement of effective range

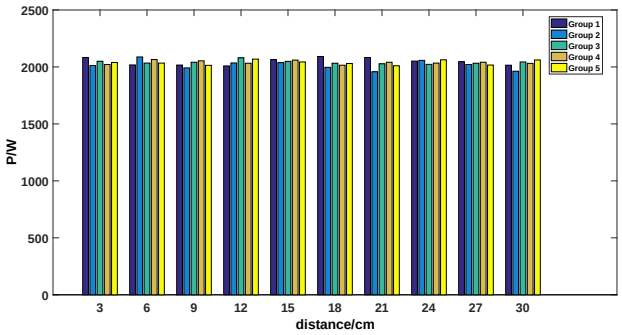

Fig. 9. The received power ditribution above the effective range

and the data collection pins are connected to the GPIO pins of the raspberryPi. It is difficult to obtain the accurate measurements due to the interference of the electromagnetic field. We therefore explore the shield approach by using the iron sheet and ground connection. In this experiment, only the distance measurement was fed to controller due to the limitation of the experiment device, as the wireless charger used in this study mainly designed for statical wireless charging, therefore power feedback control is not experimentally achievable in the current platform. The power feedback control will thus be investigated in our future study.

5.5 Control methods validation

The following disturbance

$$w_(k) = \begin{cases} 3cm : k = 10s \\ 8cm : k = 25s, k = 105s \\ -4cm : k = 45s \\ -6cm : k = 75s \\ -2cm : k = 130s \\ 0 : k = others \end{cases}$$

was introduced and the sample time was set as 10 seconds. Here the effective range is assumed to be 60 cm and the corresponding triggered condition is $[-5cm, 5cm]$ under ETC. And the range $[-1cm, 1cm]$ is chosen as the stability range instead of zero point under GSFC. This is because the distance measurement errors are about 1 cm due to the sensor precision.

The states of $\Delta d(k)$ under ETC and GSFC are shown in Fig. 10. The sequence { D_i, i=1, 2, 3, 4, 5, 6} represents disturbances, the sequence {E_i, i=1, 2, $\cdots$, 12} represents the responses for corresponding disturbance under ETC, and the sequence {G_i, i=1, 2, $\cdots$, 12} represents the responses for correponding diturbances under GSFC.

The experimental results presented above show that less control actions are taken by the event-triggered control than the general state feedback control. Indeed, it dos not neet to control when

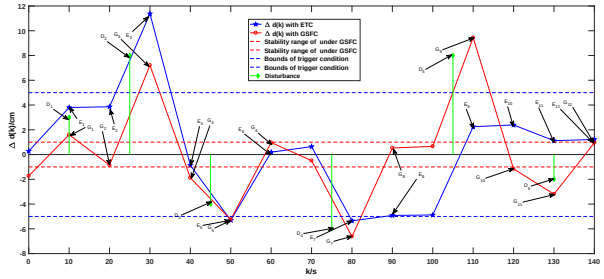

Fig. 10. $\Delta d(k)$ under different control approaches with disturbance sequence { D_i, i=1, 2, 3, 4, 5, 6} .The sequence {E_i, i=1, 2, $\cdots$, 12} represents the responses for corresponding disturbance and ETC, and the sequence {G_i, i=1, 2, $\cdots$, 12} represents the responses for correponding diturbances and GSFC.The small deviation caused by disturbance was not controlled with ETC because the trigger condition was not satisfied. On the contrary, any deviation caused by disturbance was alway controlled with GSFC.

the EV is withn the effective range because the received power above the range is almostly the same as shown in Fig. 9. The experimental results again confirm the efficacy of the proposed mobile wireless charging approach.

6 Conclusion

This paper has proposed an event-triggered switch control approach for the adjustment of the relative position between receiver coil and track coi for on-road dynamical wireless charging of EVs. The sufficient condition for searching the controller gains is developed by the means of LMI formulation. Compared to the general state feedback control, the designed controller can be triggered under different control modes according to the practical working environment, which avoids excessive control actions, thus reducing the waste of control energy in the EVs . The marginal stable mathematical model parameters are used in the numerical simulation, which are capable of reflecting the dynamic behaviour of the EVs. Finally, an EV wireless charging platform was built. The designed mechanical device not only connects the car body and receiver coil easily but also enables the easy implementation of the control algorithm.

Future work will focus on the design of dynamic wireless charging platform so that the received power can be used in the feedback control to improve the power charging efficiency.

Acknowledgments This work was supported by Shanghai Green Energy Grid Connected Technology Engineering Research Center under Grant 13DZ2251900, the Shanghai Natural Science Foundation under Grant 15ZR1417500, EPSRC iGIVE project under grant EP/L001063/1, and NSFC under grant 61673256.

Bibliography

Buja G, Bertoluzzo M and Dashora HK (2016) Lumped track layout design for dynamic wireless charging of electric vehicle. *IEEE Transactions on Industrial Electronics* 63 (10): 6631-6641.

Chen L, Nagendra GR and Boys JT (2015) Double-coupled systems for IPT roadway applications. *IEEE Journal of Emerging and Selected Topics in Power Electronics* 3 (1): 37-50.

Choi SY, Gu BW and Jeong SY(2014) Trends of wireless power transfer systems for roadway powered electric vehicles. *2014 IEEE 79th Vehicular Technology Conference* : 1-5.

Choi SY, Gu BW and Jeong SY (2015) Advances in wireless power transfer systems for roadway-powered electric vehicles. *IEEE Journal of Emerging and Selected Topics in Power Electronics* 3 (1): 18-37.

Covic GA and Boys JT (2013a) Inductive power transfer. *Proceedings of the IEEE* 101 (6): 1276-1290.

Covic GA and Boy JT (2013b) Modern trends in inductive power transfer for transportation applications. *IEEE Journal of Emerging and Selected Topics in Power Electronics* 1 (1): 28-41.

Deng WH, Kang L and Fei MR (2013) Identification and outreceivert tracking control of Hammerstein systems through wireless networks. *Transactions of the Institute of Measurement and Control* 36 (1): 3-13.

Esteban B, Sid-Ahmed M and Kar NC (2015) A comparative study of power supply architectures in wireless EV charging systems. *IEEE Transactions on Power Electronics* 30 (11): 6408-6422.

Girard A (2015) Dynamic Triggering Mechanisms for Event-Triggered Control. *IEEE Transactions on Automatic Control* 60 (7): 1992-1997.

He Y, Venkatesh B and Guan L (2012) Optimal scheduling for charging and discharging of electric vehicles. *IEEE Transactions on Smart Grid* 3 (3): 1095-1105.

Ko YD, Young D and Jang YJ (2013) The optimal system design of the online electric vehicle utilizing wireless power transmission technology. *IEEE Transactions on Intelligent Transportation Systems* 14 (3): 1255-11265.

Lee K, Pantic Z and Lukic SM (2014) Reflexive field containment in dynamic inductive power transfer systems. *IEEE Transactions on Power Electronics* 29 (9): 4592-4602.

Liu H, Huang XL, Tan LL and Guo JP (2016) Switching control optimisation strategy of segmented transmitting coils for on-road charging of electrical vehicles. *IET Power Electronics* 9 (11): 2282-2288.

Lukic S and Pantic Z (2013) Cutting the cord: static and synamic inductive wireless charging of electric vehicles. *IEEE Electrification Magazine* 1 (1): 57-64.

Miller JM (2014) Electric and hybrid vehicles-technology leaders. *IEEE Electrification Magazine* 2 (2): 4-5.

Miller JM, Jones PT and Li JM (2015) ORNL experience and challenges facing dynamic wireless power charging of EV's. *IEEE Circuits and Systems Magazine* 15 (2): 40-53.

Peng C and Ma S (2017) Observer-based non-PDC control for networked T-S fuzzy systems with an event -triggered communication. *IEEE Transactions on Cybernetics* 47 (8): 2279-2287.

Selivanov A and Fridman E (2016) Event-Triggered H_∞ Control: A Switching Approach. *IEEE Transactions on Automatic Control* 61 (10): 3221-3226.

Wayes T, Walid S and Vincent Poor H (2012) Economics of electric vehicle charging: a game theoretic approach. *IEEE Transactions on Smart Grid* 3 (4): 1767-1778.

Wang XM, Chau Y and Naveed UI (2016) Electric Vehicle Charging Station Placement for Urban Public Bus Systems. *IEEE Transactions on Intelligent Transportation Systems* 18 (1): 128-139.

Zhang H, Zheng XY and Yan HC (2017) Codesign of event-triggered and distributed H filtering for active semi-vehicle suspension systems. *IEEE Transactions on Mechatronics* 22 (2): 1047-1058.

Zaheer A, Neath M and Beh ZZ (2017) A Dynamic EV Charging System for Slow Moving Traffic Applications. *IEEE Transactions on Transportation Electrification* 3 (2): 354-369.